

Article

A Continuously Derivable Uniaxial Tensile Stress-Strain Model of Cold-Formed Circular Steels

Chang Yang, Ling Ying, Binbin Wang and Qi Li *

College of Architecture and Urban-Rural Planning, Sichuan Agricultural University, Chengdu 611830, China; 41479@sicau.edu.cn (C.Y.); yingling9898@163.com (L.Y.); wangbinbin0806@163.com (B.W.)

* Correspondence: 41471@sicau.edu.cn

Abstract: Promoting prefabricated steel structures is considered one of the crucial approaches to meeting the objectives of “carbon peak” and “carbon neutrality” in the construction industry. Due to insufficient practical experience and incomplete fine engineering techniques in civil construction, the sustainable development of prefabricated building systems in China faces many challenges. Taking steel components as an example, the design process of tubular columns does not pay enough attention to the influence of the cold-working effect on material mechanical properties, and the constitutive relationship of cold-formed steels is not clear, which will cause an engineering economic burden and may affect the judgment of catastrophic problems. To serve the refined design and meet the intelligent construction technology using the computer platform, a modified Menegotto-Pinto model using a continuously derivable function is proposed in the paper. The proposed model can successfully describe the complete stress-strain curve of cold-formed circular mild steels as long as the basic mechanical parameters of the parent material are determined. Taking into account the influence of the strength and thickness of the parent steel sheets, as well as the internal bending radius r , on the cold-rolling effect, the model can also flexibly track the elastic-plastic nonlinearity of the cold-formed materials. In addition, the research shows that the cold-rolling effect will weaken with the increase of the yield strength $f_{sy,0}$ of the parent steels and r/t ratio, and may disappear when $f_{sy,0}$ reaches 1748 MPa or the r/t ratio is approximately 60, which can be used as economic indicators during the design process.



Citation: Yang, C.; Ying, L.; Wang, B.; Li, Q. A Continuously Derivable Uniaxial Tensile Stress-Strain Model of Cold-Formed Circular Steels.

Buildings **2024**, *14*, 36. <https://doi.org/10.3390/buildings14010036>

Academic Editors: Zechuan Yu and Dongming Li

Received: 21 November 2023

Revised: 14 December 2023

Accepted: 19 December 2023

Published: 22 December 2023



Copyright: © 2023 by the authors. Licensee MDPI, Basel, Switzerland. This article is an open access article distributed under the terms and conditions of the Creative Commons Attribution (CC BY) license (<https://creativecommons.org/licenses/by/4.0/>).

Keywords: cold-formed; mild steels; circular hollow sections; uniaxial tensile stress-strain model; material property; high-strength

1. Introduction

To accomplish the objectives of “carbon peak” and “carbon neutrality” in the building and construction industries, the promotion and application of prefabricated steel structure buildings are advocated to meet the requirements of the circular economy and sustainable development in China [1,2]. The measures to promote prefabricated steel structure buildings can be divided into the following broad categories: construction technology, the use of high-strength steel, intelligent construction technology using the computer platform, and so on [3]. In recent years, due to their high capacity, ease of construction, and recyclable utilization, cold-formed steel structures have shown great potential in intelligent design. While experiencing cold-forming, the uniaxial tensile stress-strain curve of mild steels exhibits a more rounded stress-strain response which is no longer suitable to be described by an ideal elastic-plastic model or simple broken line models. However, the most popular structural design is still inclined to use such models to simulate cold-formed steels. On the other side, the guidance contents in most of the current specifications [4–6] are on the basis of early experimental work, which limits the range of material strength and geometry parameters. In fact, there are significant differences in the strength improvement of different steel section types formed through cold-rolling. Those specifications primarily concentrate

on the strength enhancement for the corner sections but neglect the cold-rolling effect for the circular hollow sections (CHSs for short). The above issues may lead to some key technical issues being vague and increasing the economic burden of engineering, which contradicts the intention of green building and intelligent design.

Determining a material constitutive model is one of the essential parts of structural analysis. Establishing an efficient computational numerical model in intelligent design requires defined material strength and a continuous function to deal with the stress-strain relationship of materials. Many studies have been carried out to study the uniaxial tensile stress-strain models of cold-formed steels as well as the strength enhancement due to cold work. Li et al. [7] have contrasted several available predictive methods of strength enhancement and found that current specifications, such as AISI [5] and Eurocode 3 [6], overestimate the cold-formed effect on corner yield strength, while the empirical methods proposed by various researchers have limitations in terms of the r/t ratio. Liu et al. [8] proposed a new method to predict the corner strength of cold-formed conventional steels based on measured data, and the method can be applicable to the yield strength $f_{sy,0}$ of parent materials, which ranges from 256 MPa to 497 MPa and the r/t ranges from 0.57 to 7.54. Masoud Kalani [9] investigated the cold work effect on the tensile behavior of thick steel plates and verified the accuracy of several available equations for predicting the average yield stress of the experimental specimens. Pham [10] investigated the G450 channel steels to better predict the strength enhancement of high-strength steels. Chen [11] conducted an investigation into the material properties of high-strength CHS steels with r/t ranging from 11.5 to 32.3 and found that the yield strength improvement rate $f_{sy}/f_{sy,0}$ of the Q460 was 1.09, while the Q960 section exhibited no increase in strength. Meng [12] discovered that tensile coupons of high-strength CHS ($f_{sy,0} = 799$ MPa, $r/t = 7\sim 29$) exhibit lower f_{su}/f_{sy} as the r/t ratio decreases. Generally, the use of high-strength material leads to a longer life span of the structure and brings cost-effectiveness [13]. However, based on experimental investigations, Chan et al. [14] found that the measured failure strain of high-strength steels cannot meet the requirements of Eurocode 3 due to the press-braking process.

Given that most research has focused on the effect of cold-forming on material strength enhancement, the influence of cold-forming on the deformation ability of steels should be given more attention and carefully introduced into the relationship between stress and strain. Based on the differences in the fabrication process, Yao et al. [15] established a finite element-based method for plastic strains, as well as residual stresses, in cold-formed steel hollow sections, but the stress-strain relationships of cold-formed steels used in the finite element model were transformed from experimental curves. Gardner [16] proposed a method to predict the strength enhancement in the corner regions of cold-formed sections by considering the plastic strains associated with the dominant stages in the fabrication process. Further, Gardner [17] improved the Ramberg-Osgood model [18] by using piecewise functions to describe the stress-strain curve of cold-formed steels, and the improved model was confirmed to have good accuracy. Similarly, Quach and Huang [19] also raised a modified Ramberg-Osgood model to describe the uniaxial tensile stress-strain curve of cold-formed steels. Based on detailed experimental testing, Li et al. [20] established a material model to simulate cold-formed high-strength steels. Note that although the above models can reflect the rounded tensile curve characteristics of cold-formed steels, their mathematical carriers are all piecewise functions, and the steel yield strength f_{sy} after cold work is required before using these models.

In summary, the cold-rolling effect of steel is generally affected by the yield strength $f_{sy,0}$, and thickness t of the parent steel sheets, the internal bending radius r , and the section shape [21,22]. The available prediction expressions used to reveal the strength enhancement and stress-strain curves of cold-formed steels were more for corner sections than for CHSs. In order to better promote the efficient, intelligent design of prefabricated steel structures, the objective of this paper is to propose a continuously derivable uniaxial tensile stress-strain model of cold-formed circular steels. The paper focuses on the influence of cold-rolling on the material properties of CHS mild steels based on the design parameters

of the parent steels. More specifically, based on the collected experimental data of CHS mild steels with a wide range of yield strength and r/t ratio, a systematic analysis was conducted on the influence of cold-rolling on the strength and deformation of different sections of slenderness. The proposed constitutive model was established by modifying the Menegotto-Pinto model [23] since the function image can reflect a complete nonlinear characteristic of cold-formed steels under uniaxial tension and exhibits a clear physical meaning. Finally, in order to demonstrate the superiority of the proposed model, comparative studies of the full range of stress-strain curves and corresponding absorption capacity were carried out with the measured curves and available models.

2. Uniaxial Tensile Stress-Strain Model Based on the Menegotto-Pinto Model

Establishing a complete stress-strain model with a unified function will enhance the design and process of intelligent platforms. Through detailed comparison and investigation, a modified Menegotto-Pinto model was raised to describe the uniaxial tensile stress-strain relationship of cold-formed CHS mild steels. In fact, the Menegotto-Pinto model was first raised to deal with the nonlinear responses of reinforced concrete members under earthquakes, and the material law of mild steels is a four-parameter model, which is described by a continuously derivable composite function [23]. In previous studies, the model was successfully improved to fit the ascending stage of the equivalent stress-strain relationship of cold-formed steel stub columns [24], and its mathematical expression and corresponding figure are shown in Equation (1) and Figure 1, respectively. Note that the parameter S , as shown in Figure 1, represents the ratio of ultimate tensile strength to yield strength. Combining Equation (1) and Figure 1, it can be seen that the modified model is composed of a derivable function and can flexibly track the material nonlinearity by adjusting the value of N .

$$f_s = E_s \varepsilon_s \left(Q + \frac{1 - Q}{\left(1 + \left(\frac{\varepsilon_s}{\varepsilon_{sy}}\right)^N\right)^{\frac{1}{N}}} \right), \quad \varepsilon_s \leq \varepsilon_{su} \quad (1)$$

where Q is the strain-hardening coefficient; the exponent N mainly controls the roundness of the yield stage; ε_{sy} is the nominal yield strain; ε_{su} is the ultimate strain corresponding to the ultimate tensile strength f_{su} .

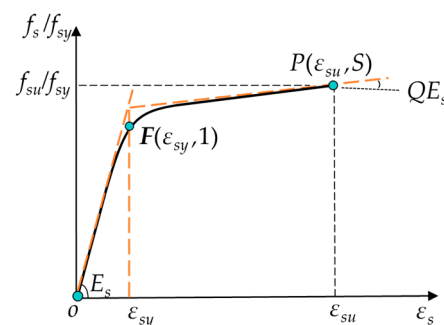


Figure 1. Outline of the improved uniaxial stress-strain model for cold-formed CHS steels based on the Menegotto-Pinto model.

To improve the efficiency of intelligent design and to highlight the relationship between the constitutive model of cold-formed mild steels and design parameters ($f_{sy,0}$ and t of the parent material and the r/t ratio of CHS), the paper intends to continue improving the modified Menegotto-Pinto model for fitting the material constitutive model of cold-formed CHS mild steels.

3. Tensile Coupon Details of Cold-Formed CHS Steels

A comprehensive collection of 74 experimental results from the available literature is assembled. Figure 2 displays the labels assigned to the tensile coupon, while specimens

from the weld area are excluded from the analysis. Additionally, specimens failing to meet the ductility requirements of the specifications are also eliminated. A summary of the variables of specimens as well as necessary experimental results is provided in Table 1, where $f_{sy,0}$ and f_{sy} are the yield strengths of the same material before and after cold-rolling, respectively. Additionally, f_{su} represents the ultimate tensile strength of cold-formed CHS steel specimens. For convenience, based on the parent steel, coupons with $f_{sy,0}$ exceeding 460 MPa are considered high-strength steels [25]. As shown in Table 1, the range of $f_{sy,0}$ is from 400 MPa to 1400 MPa, corresponding to the thickness t of steel sheets varying from 1.5 mm to 10 mm, while the yield strength improves from 357 MPa to 1402 MPa for cold-formed CHSs with a r/t ratio of 6~32.

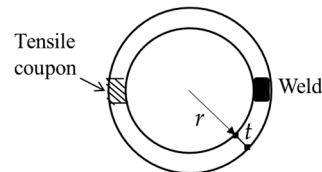


Figure 2. Location of the tensile coupon.

Table 1. Summary of the detail of tensile coupons.

Ref.	Specimens	r/t	E_s (Gpa)	$f_{sy,0}$ (MPa)	f_{sy} (MPa)	f_{su} (MPa)
[11]	4C200 × 3	32.3	207.4	546.5	571.7	632.8
	4C150 × 3	24	205.4	546.5	574.4	623.2
	4C150 × 6	11.5	217.2	580.7	623.9	694.8
	4C200 × 6	15.7	216	580.7	630.3	698.5
	4C250 × 6	19.8	217.8	580.7	603.5	685.2
	6C150 × 6	11.5	198.8	756.3	765.1	808.6
	6C200 × 6	15.7	208	756.3	758.3	808
	6C350 × 6	28.2	207.7	756.3	755.6	804.1
	9C150 × 6	11.5	205.6	973.3	959	1045.2
	9C200 × 6	19	208.3	973.3	964.7	1040.5
9C300 × 6	29	207.7	973.3	969.9	1037.1	
[12]	CHS139.7 × 4	16.6	213.3	700	742.4	842.3
	CHS168.3 × 4	20.3	211.7	700	720	823.4
	CHS139.7 × 5	13.3	212.5	700	729.7	843.3
	CHS139.7 × 6	10.6	207.9	700	779	866.7
	CHS139.7 × 8	7.9	205.7	700	784.8	866.8
	CHS139.7 × 10	6.1	205.6	700	787.6	877.5
[26]	89 × 4	10.1	209	1100	1084	1242
	108 × 4	12.5	208	1100	1233	1327
	133 × 4	15.6	210	1100	1164	1278
	89 × 3	13.8	203	900	980	1093
[27]	V89 × 4	10.4	210	900	1054	1108
	S89 × 4	10.4	205	1100	1180	1317
	S108 × 4	12.9	215	1100	1180	1292
	S133 × 4	16.1	204	1100	1159	1291
	S139 × 6	10.8	194	1100	1014	1382
	V89 × 3	14.03	209	900	1053	1124
Total	21 coupons	6.1~32.3	198.8~217.8	546.5~1100	571.7~1233	623.2~1382
[28]	CHS01	11.5	203	690	746	811
	CHS02	15.7	204	690	747	816
	CHS03	9	202	690	757	837
	CHS04	11.5	201	690	767	827

Table 1. Cont.

Ref.	Specimens	r/t	E_s (Gpa)	$f_{sy,0}$ (MPa)	f_{sy} (MPa)	f_{su} (MPa)
[29]	193.7 × 8	11.1	198.6	355	404	480
[30]	C1	8.7	191	350	454	520
	C2	11.3	220	350	416	484
	C3	15.5	204	350	453	521
	C4	18.3	200	350	430	514
	C5	19.4	204	350	379	440
	C6	22.8	207	350	357	474
	C7	23	193	350	433	479
	C8	27.5	206	350	395	481
[31]	CBC1	19.1	200	350	365	469
	CBC2	14.9	210	350	432	538
	CBC3	14.6	218	350	415	534
	CBC4	11.4	211	350	433	508
	CBC5	10.8	205	350	456	548
	CBC6	9.1	204	350	408	503
	CBC7	7.1	207	350	442	511
	CBC8	5.4	209	350	460	568
[32]	TS1A	10.7	190.9	1350	1402	1558
	TS1B	10.8	195.1	1350	1392	1533
	TS1C	10.6	190.7	1350	1400	1550
	TS2A	9.3	198.3	1350	1361	1513
	TS2B	9.4	204.4	1350	1360	1507
	TS2C	9.2	197.6	1350	1362	1499
	TS3A	8.3	195.6	1350	1328	1477
	TS3B	8.4	197.1	1350	1329	1495
	TS3C	8.3	200.2	1350	1332	1487
	TS4A	16.8	203	1350	1346	1506
	TS4B	16.6	194.2	1350	1365	1519
	TS4C	16.9	197	1350	1368	1540
	TA5A	16.9	195.2	1350	1363	1540
	TS5B	16.9	196.7	1350	1370	1568
	TS5C	22.7	203.7	1350	1399	1520
[33]	1	22.6	201.6	355	456.8	527
	2	22.9	203.6	355	451.7	534.2
	3	14	200.2	355	455.6	529.2
	4	14	195.4	355	392	503.7
	5	17.9	196.6	355	405.2	511.8
	6	17.9	198.5	355	443.9	508.1
	7	21.2	196.7	355	385	500
	8	21.2	197.3	355	397.4	511.1
	9	21.2	196.7	355	436.4	502.1
[34]	CHS139.7 × 8	8	202.2	700	856.8	893.7
	CHS139.7 × 10	6	203.1	700	762	804.9
Total	53 coupons	5.4~27.5	190.7~220	350~1350	357~1402	440~1568

Figure 3 summarizes the range of values for several key parameters of the collected tensile coupons. The coupons are divided into three groups, with the boundaries of $f_{sy,0}$ being 460 MPa and 690 MPa, respectively. As shown in Figure 3, the number of coupons for the three groups is relatively uniform, as well as the range of r/t .

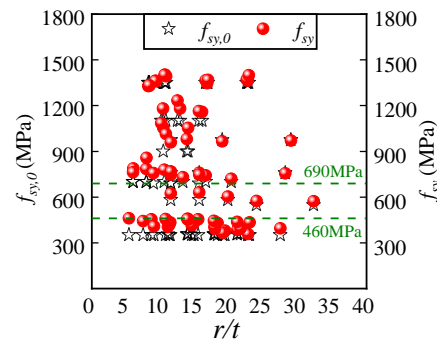


Figure 3. Distribution of the main measured variables of the collected experimental data.

All the gathered measured data are utilized to establish a predictive expression for the yield strength f_{sy} and ultimate tensile strength f_{su} considering the cold work of materials. 54 sets of experimental values of ultimate strain ε_{su} from cold-formed CHS steel specimens are used to assess the corresponding empirical formula. Furthermore, a total of 26 stress-strain curves spanning the full range are examined and analyzed to derive suitable prediction formulas for the curvature coefficient N and the strain-hardening exponent Q . The mathematical expressions of these parameters will be derived in the following sections.

4. Analysis of Results and Recommendations

4.1. Yield Strength f_{sy} of Cold-Formed CHSs

Based on the collected data of Table 1, Figure 4 presents the relationship between the measured yield strength f_{sy} and the r/t ratio, and f_{sy} has been normalized by the measured $f_{sy,0}$. According to the trend line of the red dotted line shown in Figure 4, it can be found that the $f_{sy}/f_{sy,0}$ ratio decreases with the r/t ratio increasing, and the cold-rolling effect seems to disappear when the value of the r/t ratio reaches 60 based on the trend line of Figure 4.

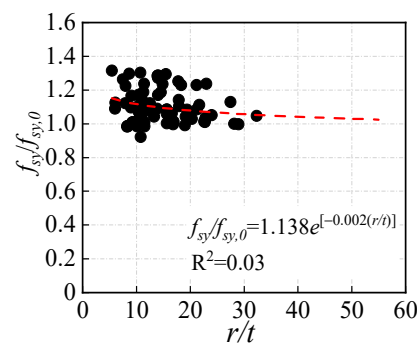


Figure 4. Relationship between the measured $f_{sy}/f_{sy,0}$ ratio and r/t .

The yield strength of the cold-formed CHS steels differs from that of the parent material. To examine the influence of the cold-rolling effect, a sensitivity analysis is conducted on the r/t ratio and the yield strengths $f_{sy,0}$ and f_{sy} . By comparing the relationship between f_{sy} and three different physical quantities shown in Figure 5, it can be found that the independent r/t is different in establishing connections with f_{sy} , while the compound parameter $f_{sy,0}/(r/t)^{0.5}$ exhibits a better correlation with f_{sy} as the R^2 reaches 0.87. The optimal group is the relationship between $f_{sy,0}$ and f_{sy} because the measured f_{sy} has the strongest correlation with $f_{sy,0}$, which can be expressed by a linear function.

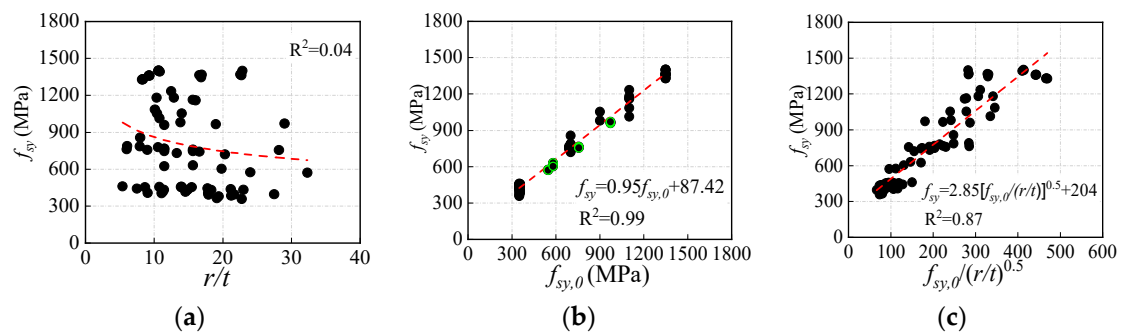


Figure 5. Relationships between the yield strength f_{sy} of CHS and the main variables. (a) r/t . (b) $f_{sy,0}$. (c) combined parameters based on r/t and $f_{sy,0}$.

The red trend line in Figure 5b shows that the relationship between $f_{sy,0}$ and f_{sy} exhibits a strong linear correlation. The difference between f_{sy} and $f_{sy,0}$ decreases and even disappears with the increase of $f_{sy,0}$, and the results is also confirmed by previous research [11], the relevant experimental data of which is highlighted in green dots in Figure 5b. Furthermore, if setting the $f_{sy}/f_{sy,0}$ ratio to 1.0, it can be obtained that the value of f_{sy} is 1748 MPa, and the value suggests that the influence of material strength on the cold-rolling effect has an upper limit. Based on the results shown above, a more physically meaningful way of determining f_{sy} can be obtained, as shown in Equation (2). When $f_{sy,0}$ exceeds 1748 MPa, the value of f_{sy} can be considered consistent with $f_{sy,0}$.

$$\frac{f_{sy}}{1748} = 0.95 \frac{f_{sy,0}}{1748} + 0.05 \quad (f_{sy,0} \leq 1748 \text{ MPa}) \quad (2)$$

4.2. Curvature Coefficient N

The curvature coefficient N is the critical roundness variable at the yield stages of the stress-strain curve. In this section, the analytical curve is required to pass through the coordinate origin and the point $(\varepsilon_{su}, f_{su})$ shown in Figure 1. The ideal value of N is evaluated based on two criteria: (1) the envelope area ratio of the calculated results A_{cal} to the experimental results A_{exp} (corresponding to Figure 6a), and (2) the coincidence degree of the transition curvature in the elastic-plastic stage (corresponding to Figure 6b). Through debugging and analysis, as shown in Figure 6, the empirical values of N are almost in the range of 4 to 8.

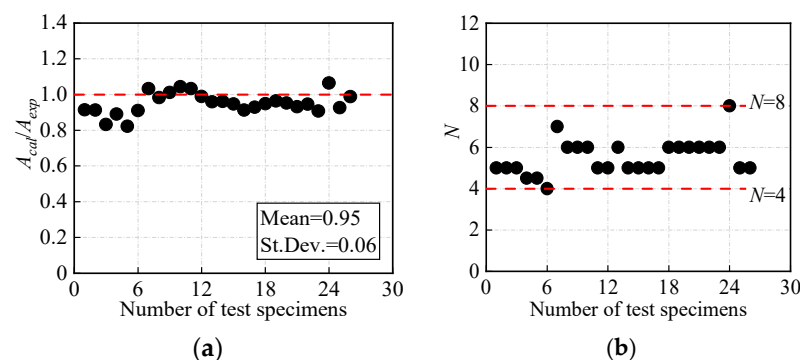


Figure 6. The value of the curvature coefficient N . (a) Optimal envelope area. (b) Optimal elastic-plastic curvature.

The relationships between the curvature coefficient N and the main variables are shown in Figure 7. It is clear that the r/t ratio and the combined parameter $f_{sy,0}/(r/t)^{0.5}$ are not the primary factors affecting the curvature coefficient N , while $f_{sy,0}$ and the corresponding strain $\varepsilon_{sy,0}$ have the same correlation coefficient relationship with N . Considering the

influence of the elastic modulus E_s of tensile coupons, $\epsilon_{sy,0}$ is chosen to be the primary factor, and Equation (3) is proposed to calculate the curvature coefficient N .

$$N = 0.33\epsilon_{sy,0}^{-0.05} = 0.33\left(f_{sy,0}/E_s\right)^{-0.5} \tag{3}$$

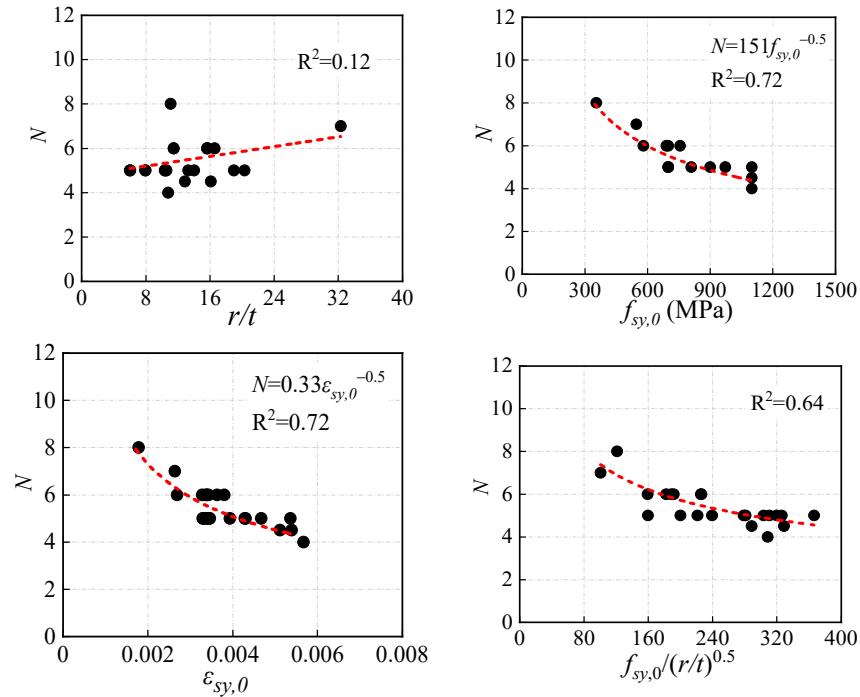


Figure 7. Relationships between the curvature coefficient N and the main variables.

4.3. Strain-Hardening Exponent Q

The strain-hardening exponent Q characterizes the strain-hardening behavior of the strengthening segment. The value of Q can be determined by defining two points (ϵ_{sy}, f_{sy}) and (ϵ_{su}, f_{su}) , as shown in Figure 1. To identify the critical factor for Q , the relationships between the measured Q and the main variables are shown in Figure 8. It can be concluded that the correlation coefficient R^2 between the combination parameter $(r/t)^2/f_{sy,0}$ and Q is 0.65, which is higher than that of the other variables. Therefore, the strain-hardening coefficient Q can be calculated using Equation (4).

$$Q = 0.0053 \left[(r/t)^2 / f_{sy,0} \right]^{-0.13} \tag{4}$$

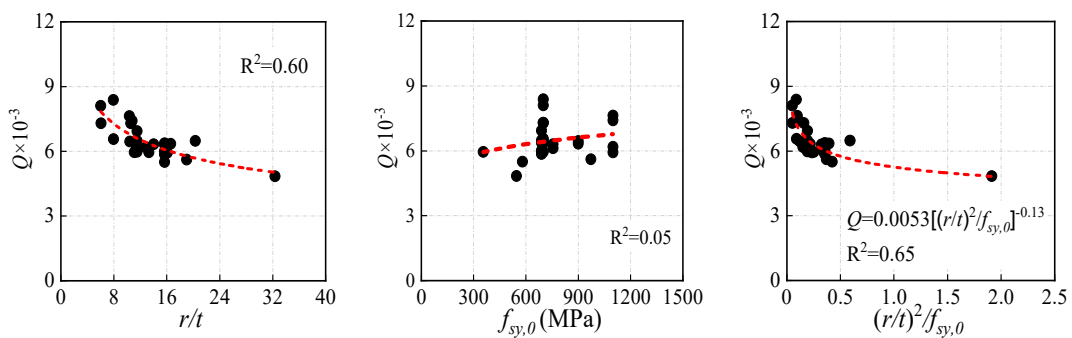


Figure 8. Relationships between the strain-hardening exponent Q and the main variables.

4.4. Ultimate Strain ε_{su}

The relationships between the ultimate strain ε_{su} and the main variables are shown in Figure 9. There is no obvious relationship between the measured ultimate strain $\varepsilon_{su,cal}$ and the r/t ratio. The correlation coefficient between ε_{su} and the $\varepsilon_{sy,0}$ is 0.82. It can be observed that the ultimate strain ε_{su} shows a stronger correlation with the combined parameter $f_{sy,0}/(r/t)^{0.5}$ compared with $\varepsilon_{sy,0}$, whose correlation coefficient is 0.9.

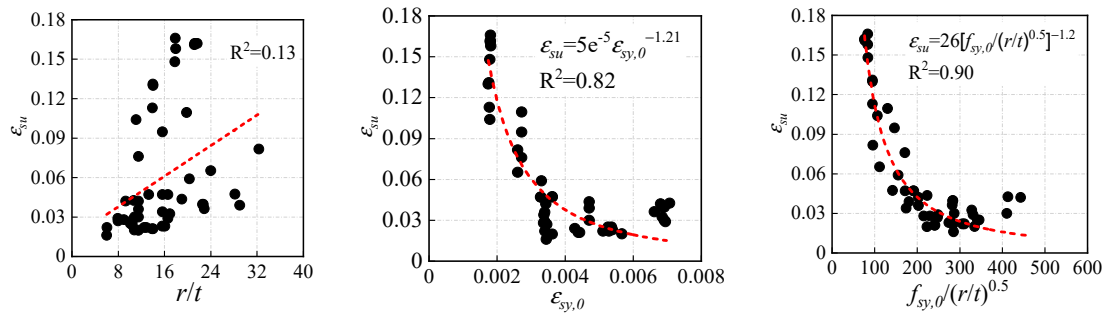


Figure 9. Relationships between the ultimate strain ε_{su} and the main variables.

To summarize, the ultimate strain ε_{su} can be calculated by the following formula:

$$\varepsilon_{su} = 26 \left[f_{sy,0} / (r/t)^{0.5} \right]^{-1.2} \quad (5)$$

4.5. Ultimate Strength f_{su}

Figure 10 shows the relationship between ultimate tensile strength f_{su} and three main factors. There is no obvious relationship between the r/t ratio and f_{su} . The correlation coefficient between f_{su} and the combined parameter is 0.87, while the strongest correlation can be observed between $f_{sy,0}$ and f_{su} with a correlation coefficient as high as 0.99, which implies an extremely strong linear correlation.

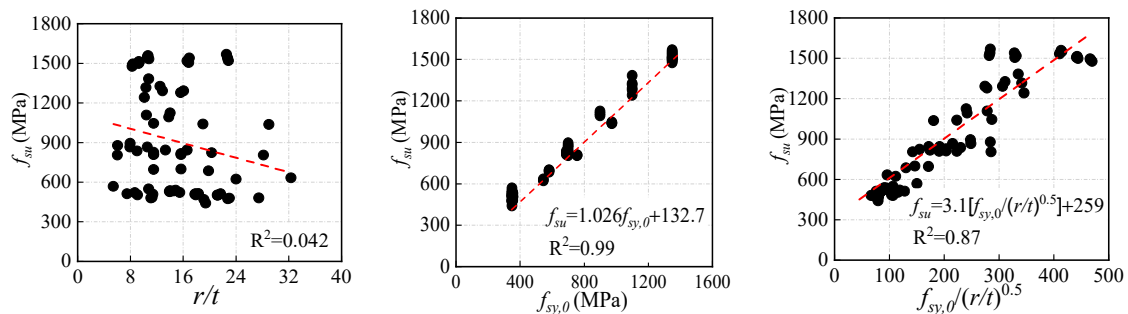


Figure 10. Relationships between the ultimate strength f_{su} and the main variables.

By comparing the relationship between f_{su} and three different physical quantities shown in Figure 10, it can be found that the optimal group is the linear relationship between $f_{sy,0}$ and f_{su} . This indicates that there is a significant correlation between the yield strength of the parent steels and f_{sy} compared with other factors, and the following equation is derived to calculate the ultimate tensile strength:

$$f_{su} = 1.026f_{sy,0} + 132.7 \quad (6)$$

5. Verification of the Proposed Model

5.1. Comparison of the Calculated Results and Measured Results

Comparisons between the experimental and calculated results are conducted, including ultimate tensile strength f_{su} , ultimate strain ε_{su} , and uniaxial tensile stress-strain curves of cold-formed steels. Firstly, the experimental ultimate strain of 54 groups of specimens

is compared with the calculated results $\varepsilon_{su,cal}$ based on both Equation (5) and the method by Gardner [17]. As shown in Figure 11, the proposed method by Equation (5) can better predict the actual results by Gardner than the method proposed by Gardner (the corresponding equations can be found in Appendix A), because its mean $\varepsilon_{su,cal}/\varepsilon_{su,exp}$ of 1.079 and moderate standard deviation of 0.3400 are both smaller than the other.

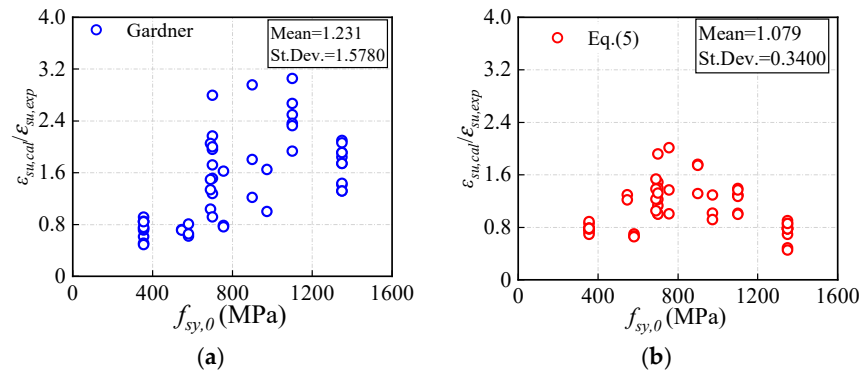


Figure 11. Comparison between the measured and calculated ultimate strain ε_{su} . (a) Available method raised by Gardner. (b) Proposed method in the paper

Secondly, the comparison between the experimental ultimate tensile strength $f_{su,exp}$ (from 74 test groups) and the calculated results $f_{su,cal}$ (obtained using Equation (6)) is conducted, as illustrated in Figure 12. The predictive expression of ultimate strength f_{su} proposed by Gardner is also plotted in the figure. Both expressions proposed demonstrate relatively high accuracy in predicting the ultimate tensile strength with errors of approximately 15%, while Equation (6) proposed by the authors is better suited for high-strength steels.

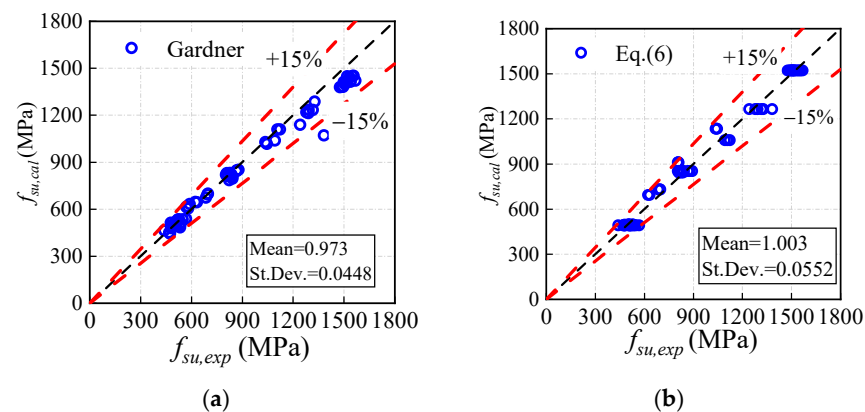


Figure 12. Comparisons between the measured and calculated ultimate strength f_{su} . (a) Available method raised by Gardner. (b) Proposed method in the paper

It is crucial to elucidate the difference between the stress-strain relationship prediction models. In order to evaluate the overall accuracy of the proposed model, a comparison is made between the measured stress-strain curves of tensile coupons and the corresponding calculated ones. Similarly, as a representative of existing models, the improved Ramberg-Osgood model proposed by Gardner is still being compared. Table 2 lists the main variables of the chosen specimens. As shown in Figure 13, both of the predictive models for cold-formed CHS steels have good consistency. Concretely, when $f_{sy,0}$ is within 600 MPa, as shown in Figure 13a,b, the proposed model based on the Megenetto-Pinto model is almost better than the one based on the Ramberg-Osgood model. With the value of $f_{sy,0}$ increasing, as shown in Figure 13c, the two models are seen to have consistent accuracy. However, it should be noted that the improved Megenetto-Pinto model proposed in the paper is

directly based on the most basic design parameters, including $f_{sy,0}$ and t of the parent steels and internal bending radius r , while the model proposed by Gardner needs to know the yield strength of cold-formed steel.

Table 2. Main variables of the test specimens for comparison.

Notation	193.7 × 8	4C200 × 3	4C200 × 6	CHS168.3 × 4	CHS139.7 × 5	6C200 × 6	6C150 × 6	9C200 × 5
$f_{sy,0}$ (MPa)	355	546.5	580	700	700	756.3	756.3	973
r/t	11.1	32.2	15.7	20.3	13.3	15.7	15.7	15
Ref.	[29]	[11]		[12]			[11]	

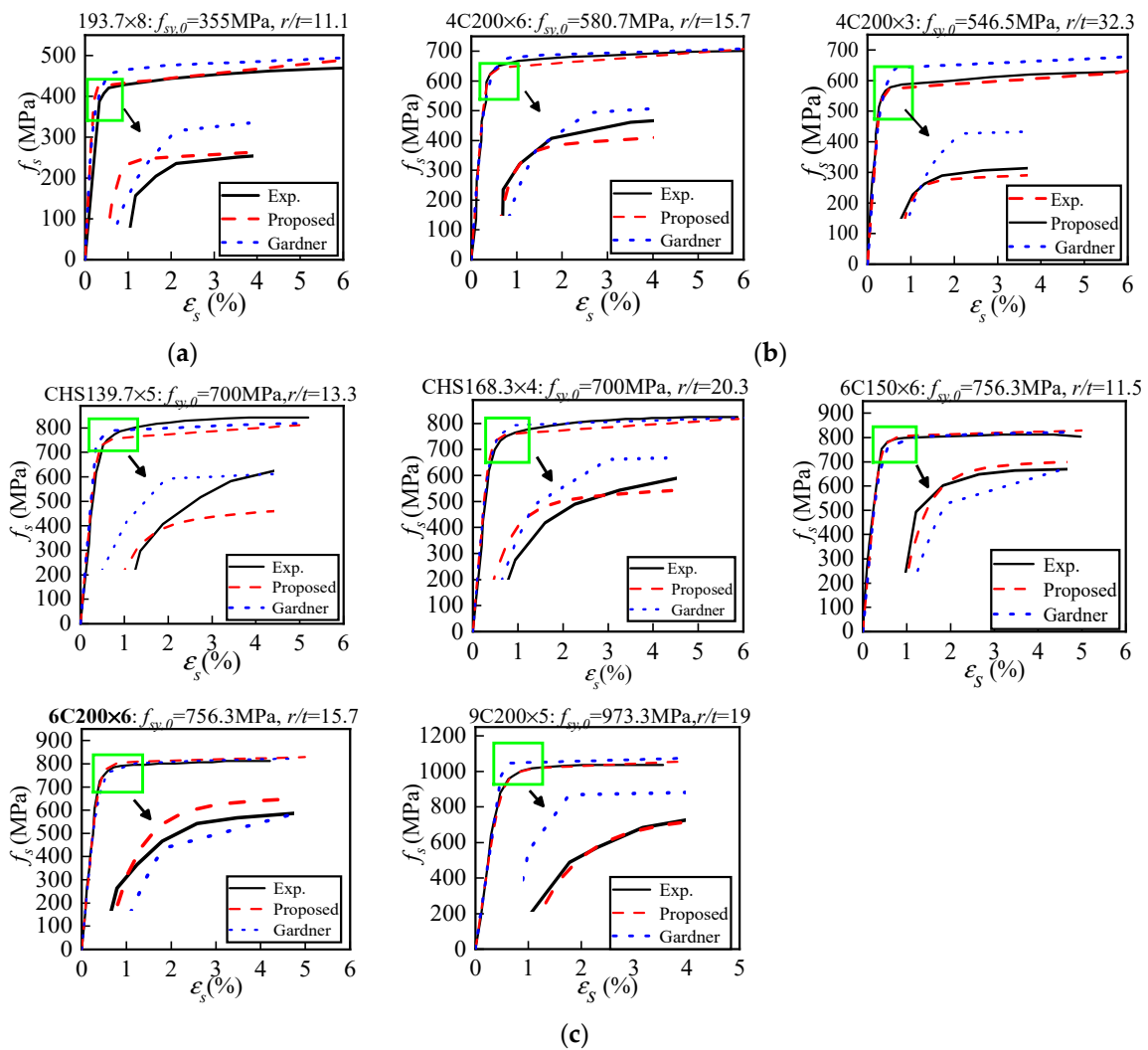


Figure 13. Comparison of experimental and calculated uniaxial tensile stress-strain curves. (a) Conventional strength steels. (b) High-strength steels with an average $f_{sy,0}$ of 565 MPa. (c) Ultra-high strength steels with $f_{sy,0}$ greater than 690 MPa

5.2. Case Application Analysis

Choosing the cold-formed CHS steel stub columns under axial load as simulated subjects, a comparison of energy absorption, which is gained from the load-bearing curves, are carried out based on 0material constitutive models of the ideal elastoplastic model and the modified model, respectively. The energy absorption can be obtained by Equation (7). The higher the value, the stronger the ability of the component to resist deformation will become.

$$E = \int_0^D F(s)ds \quad (7)$$

where E represents the energy absorbed by the component through the entire ascending stage; $F(s)$ is the load; and D is the displacement corresponding to the load.

Table 3 shows the main variables of the numerical examples, in which the thickness t is 3 mm, the r/t ratio varies from 10 to 60, and the range of $f_{sy,0}$ is 235 MPa to 1900 MPa. Figure 14 shows the ultimate energy absorption of the total numerical examples. It can be seen that the energy absorption is often underestimated for the specimens without considering the cold-rolling effect. For the example specimens with $f_{sy,0}$ of 235 MPa shown in Figure 14a, the energy absorption capacity obtained by using the proposed model is twice that of using the ideal elastoplastic model. However, the difference in the energy absorption capacity caused by the two models decreases with $f_{sy,0}$ increasing. When the value of $f_{sy,0}$ is 960 MPa and the r/t ratio is about 60, the cold-rolling effect has little influence on the energy absorption. As $f_{sy,0}$ reaches 1800 MPa, the influence of material models seems to disappear regardless of the value of r/t .

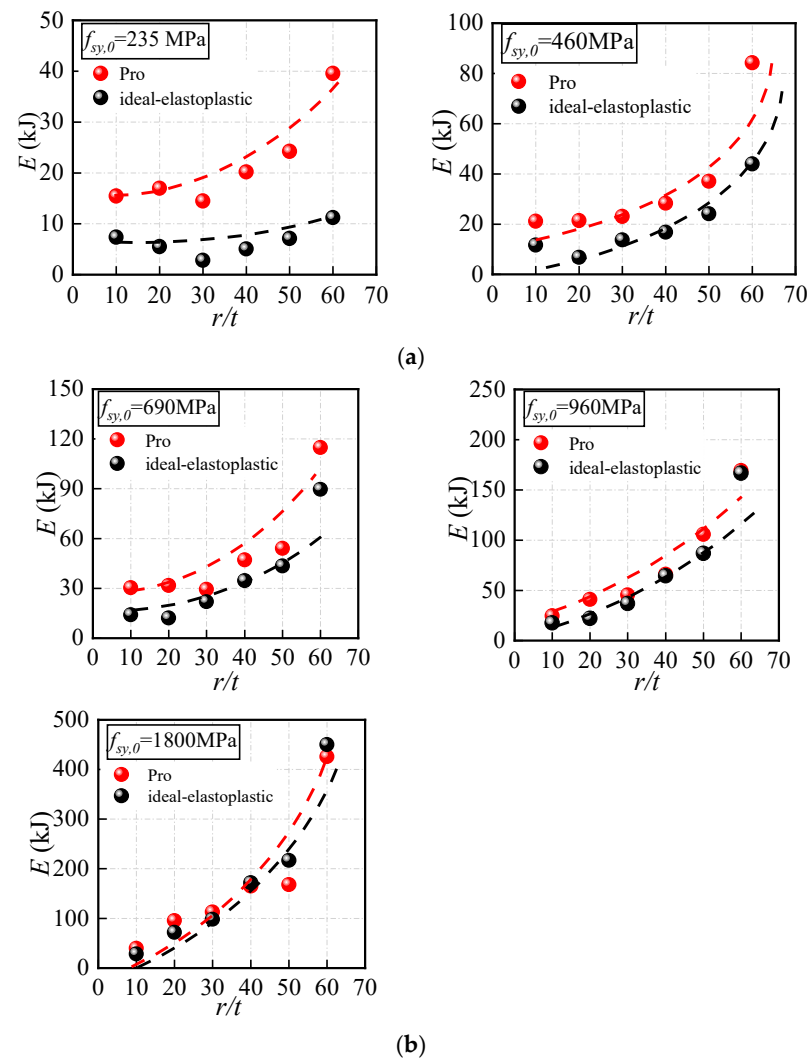


Figure 14. Energy absorption of numerical examples using different material constitutive models. (a) Conventional strength steels within 460 MPa. (b) High-strength steels exceeding 690 Mpa.

Overall, the consistency between the calculated results and measured results shows that the proposed model can be used as a digital platform for intelligent construction. In addition, compared with the ideal elastoplastic model, the proposed model established in

this paper has more distinct material properties and can more accurately evaluate the ultimate bearing capacity and corresponding deformation of the components to achieve energy saving, which is beneficial to the sustainable development of prefabricated steel buildings.

Table 3. Main variables of the numerical examples.

Sets	$f_{sy,0}$ (MPa)	t (mm)	r/t	L (mm)
1	235, 460, 690, 960, 1800	3	10	198
2	235, 460, 690, 960, 1800	3	20	378
3	235, 460, 690, 960, 1800	3	30	558
4	235, 460, 690, 960, 1800	3	40	738
5	235, 460, 690, 960, 1800	3	50	918
6	235, 460, 690, 960, 1800	3	60	1098

6. Conclusions

In order to provide a unified and efficient material constitutive model for the digital intelligent design, a continuously derivable function based on the Menegotto-Pinto model is proposed to describe a complete uniaxial tensile stress-strain relationship for cold-formed circular mild steel. The key physical quantities and auxiliary parameters of the proposed model can be calibrated once the r/t ratio of CHSs, thickness t and yield strength $f_{sy,0}$ of parent steels are determined.

To verify the validity and accuracy of the proposed model, 74 sets of experimental data on mild steel have been collected. Through comparisons between the measured results and the calculated ones, the following conclusions can be drawn:

- (1) The proposed model can predict the complete uniaxial tensile stress-strain behavior of cold-formed circular steels with high accuracy. Considering the wide varying range of the collected experimental variables such as $f_{sy,0}$ (400~1400 MPa), and r/t (5.4~32.3), the good agreement observed between the predictive and measured stress-strain curves indicates that the improved Menegotto-Pinto model proposed in this paper has a wide application scope.
- (2) The ultimate tensile strain ε_{su} of cold-formed circular steels can be predicted by Equation (5) with more improved accuracy than the model proposed by Gardner, due to the comprehensive consideration of the influence of $f_{sy,0}$ and r/t .
- (3) The cold-rolling effect that causes strength enhancement will weaken with $f_{sy,0}$ and r/t increasing and seems to be neglected when $f_{sy,0}$ reaches 1748 MPa or the r/t ratio is approximately 60.
- (4) Compared with the ideal elastoplastic model, the proposed model can more accurately estimate the load-bearing capacity of the components under extreme loads, which reduces the economic burden of engineering.

Based on the mathematical and statistical analysis process presented in the paper, the proposed material constitutive model has reparability to a certain degree, which can also be a helpful tool to develop more models for the CHS and CFST members for analyzing catastrophic engineering problems. The related studies will be reported in the near future.

Author Contributions: Conceptualization, C.Y., L.Y. and Q.L.; methodology, C.Y. and L.Y. software, C.Y. and L.Y.; analysis, C.Y., L.Y., B.W. and Q.L.; writing—original draft preparation, L.Y.; writing—reviewing and editing, C.Y. and L.Y.; supervision, C.Y., B.W. and Q.L. All authors have read and agreed to the published version of the manuscript.

Funding: This work is supported by the Opening Project of Sichuan Province University Key Laboratory of Bridge Non-destruction Detecting and Engineering Computing (Grant No. 2021QZJ02 and 2019OYJ01).

Data Availability Statement: Data is contained within the article.

Conflicts of Interest: The authors declare no conflict of interest.

Appendix A

Uniaxial tensile stress-strain model of cold-formed steels including the mathematical expressions for the ultimate tensile strength f_{su} and the corresponding strain ε_{su} proposed by Gardner [17] are expressed by Equations (A1)–(A3), respectively. Note that the models are based on the available experimental specimens with $f_{sy,0}$ of 235~1100 MPa.

$$\varepsilon_s = \begin{cases} \frac{f_s}{E_s} + 0.002 \left(\frac{f_s}{f_{sy}} \right)^n, & f_s \leq f_{sy} \\ \frac{f_s - f_{sy}}{E_{0.2}} + \left(\varepsilon_{su} - \varepsilon_{0.2} - \frac{f_{su} - f_{sy}}{E_{0.2}} \right) \left(\frac{f_s - f_{sy}}{f_{su} - f_{sy}} \right)^m + \varepsilon_{0.2}, & f_{sy} < f_s \leq f_{su} \end{cases} \quad (\text{A1})$$

$$\varepsilon_{su} = 0.6(1 - f_{sy}/f_{su}) \quad (\text{A2})$$

$$f_{su} = 1 + (130/f_{sy})^{1.4} \quad (\text{A3})$$

References

- Guiding Opinions of the General Office of the State Council on Vigorously Developing Prefabricated Buildings; State Council Bulletin of the People's Republic of China; The State Council: Beijing, China, 2016; pp. 24–26. (In Chinese)
- GB/T 51232-2016; Prefabricated Steel Structure Building Technical Standards. China Construction Industry Press: Beijing, China, 2016. (In Chinese)
- Li, Q.W.; Yue, Q.R.; Feng, P.; Xie, N.; Liu, Y. Development Status and Prospect of Steel Structure Industry Based on Carbon Peak and Carbon Neutrality Target. *Prog. Steel Build. Struct.* **2022**, *24*, 1–6+23. (In Chinese)
- GB 50017-2017; Standard for Design of Steel Structures. Ministry of Housing Urban-Rural Construction of the People's Republic of China: Beijing, China, 2017.
- AISI S100-16; North American Specification for the Design of Cold-Formed Steel Structural Members. American Iron and Steel Institute: Washington, DC, USA, 2016.
- EN 1993-1-12; Eurocode 3: Design of Steel Structures-Part 1-12: Additional Rules for the Extension of EN 1993 up to Steel Grades S 700. European Committee for Standardization (CEN): Brussels, Belgium, 2007.
- Li, C.L.; Yuan, H.; Hong, H.P. Predicting yield strength of cold-formed carbon steel: A review and new approaches. *J. Constr. Steel Res.* **2023**, *206*, 107926. [\[CrossRef\]](#)
- Liu, H.X.; Chen, J.; Chan, T.M. Predictive methods for material properties of cold-formed conventional steels in the corner region. *Thin-Walled Struct.* **2023**, *187*, 110740. [\[CrossRef\]](#)
- Kalani, M.; Bakhshi, A. Investigation of cold work effect, Karren (AISI) and ECCS (Euro Code3) equations validity and tension failure modes in thick plate cold-formed steel angle sections. *Structures* **2023**, *57*, 105092. [\[CrossRef\]](#)
- Pham, C.H.; Trinh, H.N.; Proust, G. Effect of manufacturing process on microstructures and mechanical properties, and design of cold-formed G450 steel channels. *Thin-Walled Struct.* **2021**, *162*, 107620. [\[CrossRef\]](#)
- Chen, J.B.; Chan, T.M. Material properties and residual stresses of cold-formed high-strength-steel circular hollow sections. *J. Constr. Steel Res.* **2020**, *170*, 106099. [\[CrossRef\]](#)
- Meng, X.; Gardner, L. Cross-sectional behaviour of cold-formed high strength steel circular hollow sections. *Thin. Wall. Struct.* **2020**, *156*, 106822. [\[CrossRef\]](#)
- Javidan, F.; Heidarpour, A.; Zhao, X.L.; Minkinen, J. Application of high strength and ultra-high strength steel tubes in long hybrid compressive members: Experimental and numerical investigation. *Thin-Walled Struct.* **2016**, *102*, 273–285. [\[CrossRef\]](#)
- Liu, J.Z.; Fang, H.; Chan, T.M. Experimental investigations on material properties and stub column behavior of high strength steel irregular hexagonal hollow sections. *J. Constr. Steel Res.* **2022**, *196*, 107343. [\[CrossRef\]](#)
- Yao, Y.; Quach, W.M.; Young, B. Finite element-based method for residual stresses and plastic strains in cold-formed steel hollow sections. *Eng. Struct.* **2019**, *188*, 24–42. [\[CrossRef\]](#)
- Rossi, B.; Afshan, S.; Gardner, L. Strength enhancements in cold-formed structural sections—Part II: Predictive models. *J. Construct. Steel Res.* **2013**, *83*, 189–196. [\[CrossRef\]](#)
- Gardner, L.; Yun, X. Description of stress-strain curves for cold-formed steels. *Constr. Build. Mater.* **2018**, *189*, 527–538. [\[CrossRef\]](#)
- Ramberg, W.; Osgood, W.R. *Description of Stress-Strain Curves by Three Parameters*; National Advisory Committee for Aeronautics: Washington, DC, USA, 1943.
- Quach, W.; Huang, J. Stress-strain models for light gauge steels. *Procedia Eng.* **2011**, *14*, 288–296. [\[CrossRef\]](#)
- Li, G.W.; Wu, Z.X.; Wen, D.H.; Shao, J.F.; Hu, C.X. Experimental investigation on the cold-forming effect of high strength cold-formed steel sections. *Structures* **2023**, *58*, 105615. [\[CrossRef\]](#)
- Chajes, A.; Britvec, S.; Winter, G. Effects of cold-straining on structural sheet steels. *J. Struct. Div.* **1963**, *89*, 1–32. [\[CrossRef\]](#)
- Bui, Q.; Ponthot, J. Numerical simulation of cold roll-forming processes. *J. Mater. Process. Technol.* **2008**, *202*, 275–282. [\[CrossRef\]](#)
- Menegotto, M.; Pinto, R.E. Method of analysis for cyclically loaded RC plane frames including changes in geometry and non-elastic behavior of elements under combined normal force and bending. In *IABSE Symposium on Resistance and Ultimate Deformability of Structures Acted on by Well Defined Repeated Loads*; IABSE: Zurich, Switzerland, 1973; Volume 13, pp. 15–22.

24. Yang, C.; Zhao, H.; Sun, Y.P.; Zhao, S.C. Compressive stress-strain model of cold-formed circular hollow section stub columns considering local buckling. *Thin-Walled Struct.* **2017**, *120*, 495–505. [[CrossRef](#)]
25. Ban, H.Y.; Shi, G.; Shi, Y.J.; Wang, Y.Q. Research progress on the mechanical property of high strength structural steels. *Adv. Mater. Res.* **2011**, *250*, 640–648. [[CrossRef](#)]
26. Su, M.; Cai, Y.; Chen, X.; Young, B. Behaviour of concrete-filled cold-formed high strength steel circular stub columns. *Thin-Walled Struct.* **2020**, *157*, 107078. [[CrossRef](#)]
27. Ma, J.L.; Chan, T.M.; Young, B. Material properties and residual stresses of cold-formed high strength steel hollow sections. *J. Constr. Steel Res.* **2015**, *109*, 152–165. [[CrossRef](#)]
28. Hu, Y.F.; Xiao, M.; Chung, K.; Ban, H.; Nethercot, D.A. Experimental investigation into high strength S690 cold-formed circular hollow sections under compression. *J. Constr. Steel Res.* **2022**, *194*, 107306. [[CrossRef](#)]
29. McCann, F.; Gardner, L.; Kirk, S. Elevated temperature material properties of cold-formed steel hollow sections. *Thin-Walled Struct.* **2015**, *90*, 84–94. [[CrossRef](#)]
30. Elchalakani, M.; Zhao, X.L.; Grzebieta, R. Tests on concrete filled double-skin (CHS outer and SHS inner) composite short columns under axial compression. *Thin-Walled Struct.* **2002**, *40*, 415–441. [[CrossRef](#)]
31. Elchalakani, M.; Zhao, X.L.; Grzebieta, R.H. Concrete-filled circular steel tubes subjected to pure bending. *J. Constr. Steel Res.* **2001**, *57*, 1141–1168. [[CrossRef](#)]
32. Jiao, H.; Zhao, X.L. Material ductility of very high strength (VHS) circular steel tubes in tension. *Thin-Walled Struct.* **2001**, *39*, 887–906. [[CrossRef](#)]
33. Sadowski, A.J.; Wong, W.J.; Li, S.C.S.; Málaga-Chuquitaype, C.; Pachakis, D. Critical buckling strains in thick cold-formed circular-hollow sections under cyclic loading. *J. Struct. Eng.* **2020**, *146*, 04020179. [[CrossRef](#)]
34. Zhong, Y.; Zhao, O. Experimental and numerical studies on post-fire behaviour of S700 high strength steel circular hollow sections under combined compression and bending. *Thin-Walled Struct.* **2022**, *181*, 110004. [[CrossRef](#)]

Disclaimer/Publisher’s Note: The statements, opinions and data contained in all publications are solely those of the individual author(s) and contributor(s) and not of MDPI and/or the editor(s). MDPI and/or the editor(s) disclaim responsibility for any injury to people or property resulting from any ideas, methods, instructions or products referred to in the content.